



H₂ Production from NH₃ in a BaTiO₃ Moderated Ferroelectric Packed-Bed Plasma Reactor

M. Ruiz-Martín^{1,2} · S. Marín-Meana^{1,2} · A. Megías-Sánchez^{1,2} · M. Oliva-Ramírez^{1,2} · J. Cotrino^{1,2} · A. R. González-Elipe¹ · A. Gómez-Ramírez^{1,2}

Received: 7 July 2023 / Accepted: 3 November 2023 / Published online: 23 November 2023
© The Author(s) 2023

Abstract

Plasma decomposition reactions are used for various gas phase chemical processes including the decomposition of ammonia. In this work we show that pure ammonia can be effectively decomposed at atmospheric pressure and ambient temperature using a packed-bed plasma reactor moderated with BaTiO₃ ferroelectric pellets without catalyst. The decomposition rate and energy efficiency of this ferroelectric barrier discharge reactor have been monitored as a function of applied voltage (up to a maximum value of 2.5 kV) and flow rate. For each operating condition reaction efficiencies have been correlated with the parameters defining the electrical response of the reactor. It is found that plasma current and volume inside the reactor and hence the energy efficiency of the process and the decomposition rate vary with the applied voltage and the flow of ammonia (a maximum decomposition rate of 14% and an energy efficiency of 150 LH₂/kWh has been determined under optimized operation conditions). The role of back reactions (i.e. N₂ + 3H₂ → 2NH₃) in decreasing reactor performance is another key effect affecting the overall efficiency for the ammonia decomposition. The possibilities of ferroelectric barrier discharge reactors to induce the decomposition of ammonia and the importance of keeping the operating temperature below the Curie temperature of the ferroelectric material are highlighted.

Keywords H₂ production · NH₃ decomposition · Atmospheric pressure plasma · Packed-bed plasma reactors · Back or reverse reactions · Microdischarges

Introduction

The shortages in the use of fossil fuels in line with the current policies to reduce the emission of greenhouse gases are encouraging the search for new energy vectors [1]. The procedures for their generation must be sustainable and compatible with a distributed

✉ A. Gómez-Ramírez
anamgr@us.es

¹ Laboratory of Nanotechnology on Surfaces and Plasma, Instituto de Ciencia de Materiales de Sevilla (CSIC-Universidad de Sevilla), Avda. Américo Vespucio 49, 41092 Seville, Spain

² Departamento de Física Atómica, Molecular y Nuclear, Universidad de Sevilla, Avda. Reina Mercedes, 41012 Seville, Spain

operation based on small plants and reliable transportation networks. The European Green Deal aims at archiving net zero CO₂ emissions by 2050 and a reduction of 55% by 2030 [2]. Within this transition scenario, Power-to-X technologies are expected to generate energy carriers (hydrogen or hydrogen-rich gases) using electricity generated by renewable power plants [3]. Up to now, H₂ has been the most widely investigated carrier due to its wide range of applications in different sectors. However, its complex storage and transport requirements have thrusted the search for alternative H₂-carriers, such as methanol, formic acid, liquid organic hydrogen carriers –LOHC– or ammonia [4–6]. NH₃ is a particularly interesting because its decomposition gives rise to hydrogen and nitrogen as unique by-product.

The NH₃ decomposition process is favourable at low pressures and high temperatures. The binding energy of the NH₃ molecule is 388 kJ/mol and the H molar content represents 75% of the atomic molar per molecule (weight percentage 17.7%). Besides these energy-related magnitudes, ammonia has additional advantages: it is one of the three most frequently transported chemical compounds in the world, it is produced on a large scale (230 Mt per year) [7], is neutral or has a low impact as a greenhouse gas and its storage is relatively cheap and safe.

There are different technologies to produce hydrogen from NH₃ molecules. These include thermal decomposition (at temperatures around 500 °C using catalysts containing cobalt, nickel or iron) [8], pyrolysis (usually operated at temperatures above 700 °C) [9], liquid NH₃ electrolysis [10] or decomposition with mechanochemical methods [11]. Other procedures operated at mild conditions include its decomposition assisted by electric fields [12] or by plasmas operated at atmospheric pressure. The latter has already demonstrated its effectiveness in different gas processes [13–15], including the reforming of hydrocarbons [16, 17] the elimination of contaminants [18] and the synthesis of NH₃ [19–23]. Among the available plasma technologies (gliding arc, microwaves...), packed-bed plasma reactors have been much studied due to their easy operation and large prospects of use. Packed-bed reactors work at atmospheric pressure and require relatively low voltages for plasma ignition. These conditions are very advantageous for on-board applications in cars, trucks and other vehicles.

Several experimental and theoretical studies have dealt with the plasma-assisted H₂ production using ammonia as fed gas [21, 22, 24–31]. Some works have reported the use of mixtures of NH₃ plus other gases acting as dilutants or to protect against the corrosive effects of the ammonia [30, 31]. Most frequently utilized gas carriers are N₂ and H₂ since they are the products of the reaction and would naturally be present in gas mixtures scale-up feeding plasma reactors. Akiyama et al. obtained a 100% hydrogen yield using a diluted mixture of NH₃ and N₂ containing 4.87% of the former [30]. Bang et al. used a fix mixture of 1 mol % of NH₃ diluted in N₂ and obtained a conversion of NH₃ of around 15% working at high temperatures. These authors proposed different reaction mechanisms and developed a model to account for their observations, but claimed that improvements are still needed in the process [31].

A rather common approach by the use of packed bed plasma reactors is the incorporation of catalysts to promote certain surface reactions contributing to the decomposition of ammonia [12, 27, 28, 32]. Very often, the same catalysts used for the synthesis of ammonia are used for their decomposition. Yi et al. used both nanometallic and bimetallic catalysts of Fe, Co, Ni and Mo for the decomposition process, and found practically a 100% of conversion at 500 °C, the decomposition notably diminishing when decreasing the temperature [27]. Wang et al. also found an improvement of the conversion when adding a Fe-catalyst at temperatures above 380 °C [28]. They found a NH₃ conversion close to

100% working at 410 °C and pointed out a relevant effect on the ammonia excited species involved in the decomposition process [26]. Working at room temperature, Andersen et al. analysed the effect of different catalyst supports and found a maximum conversion of 15% for MgAl_2O_4 . They prove the important role of the microdischarges in the decomposition process, as well as the existence of a linear correlation between the dielectric constant of the packed material and the conversion degree [29]. Hayakawa et al. developed a two-step approach in which they combined a catalytic reactor operating at approximately 700 °C with a plasma membrane reactor. This innovative method yielded a pure hydrogen flow rate of 120 L/h [25], whereas solely employing the plasma membrane reactor resulted in a flow rate of 20 ml/min [24]. In plasma-catalyst reactors the enhancement in the ammonia decomposition yield has been generally attributed to the contribution of reactions at the catalyst surface. However, the importance of such surface reactions within the overall process is currently under discussion. The controversy stems from recent investigations reporting that surface catalytic reactions are second order or even negligible and that bulk-plasma processes determine the main reaction pathways leading to the formation of the desired chemical products [21, 32].

In this work, we study the H_2 production by decomposition of pure NH_3 in a packed-bed plasma reactor, using BaTiO_3 as discharge moderator, but no specific catalyst or carrier gas to dilute the ammonia. For the sake of precision, we designate this type of reactor as ferroelectric barrier discharge (FBD). These reactors may generate quite intense plasmas at relatively low excitation voltages and frequencies [33]. In the current work, the excitation voltage and the gas flow rate were selected as running parameters to optimise the reactor performance. The decomposition degree of ammonia and the energy efficiency of the process have been related with the expansion of plasma volume within the reactor and the characteristics of the discharge as determined by an exhaustive electrical characterization of the plasma reaction under different operation conditions. The results obtained reveal that the inlet flow is a critical factor that, affecting the electrical properties of the discharge, enables the adjustment of both the amount of produced H_2 and the energy efficiency of the process. Our results also provide some hints about the occurrence of detrimental reactions (i.e., back formation of ammonia) and the conditions favouring them. Although additional research is still required, the results reported here highlight the importance of plasma microdischarges, its distribution within the reactor volume and its dependence on simple running parameters such as flow rates for an effective control of ammonia reactivity and final decomposition degree.

Experimental

Figure 1 shows a sketch of the packed-bed plasma reactor utilized in this work. A similar reactor has been previously used for the synthesis of ammonia, CO_2 elimination and various revalorization reactions [15, 17, 21, 22, 34, 35]. It consists of a cylindrical stainless steel chamber containing two circular aluminium electrodes (7.5 mm in diameter), separated by a 5 mm gap. The ground electrode is placed at the bottom of the chamber. It has a hole in its centre that acts as gas inlet. Gas outlet tube and active electrode are placed on the lid of the cylindrical chamber, this latter also made of stainless steel. The inter-electrode space was filled with rounded barium titanate (BaTiO_3) pellets, with a mean diameter of 2–3 mm. The fraction of voids in the packed-bed barrier has been estimated in 36–42%. The morphological properties of the packed bed

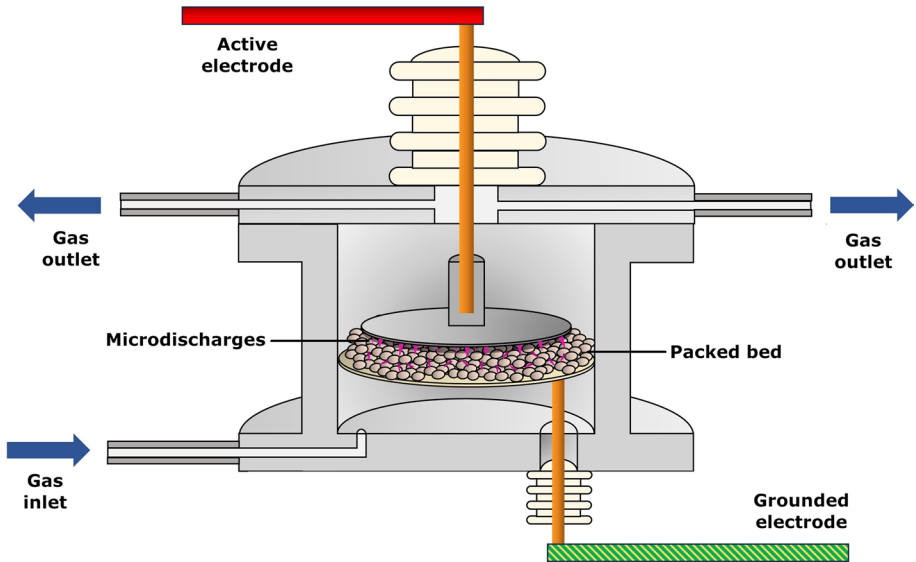


Fig. 1 Sketch of the packed-bed plasma reactor

material, as well as a photograph of the reactor, are provided as supplementary material S1. All experiments were carried out at atmospheric pressure and room temperature, using pure ammonia as input gas. Experiments were repeated three times. To analyse the effect of residence time on process performance, the total flow rate of NH_3 was varied between 4.5 and 25 sccm using a mass flow controller (Bronkhorst, EL-flow type). A Fourier transform infrared spectrometer (FTIR) located downstream the reactor was used to quantitatively determine the composition of the exit gas mixture (the device was calibrated previously with mixtures of NH_3 , H_2 , and N_2 in different proportions). Each FTIR measurement is an average of 6 individual measurements.

To ignite the plasma, the active electrode was connected by means of an electrical feedthrough to a high voltage amplifier (Trek, Model PD05034) and a function generator (Stanford Research System, Model DS345). A sinusoidal $V(t)$ signal waveform was used for electrical excitation. The excitation signal was characterized by a constant frequency of 5 kHz and a voltage amplitude varying from 1.5 to 2.5 kV. $I(t)$ and $V(t)$ curves were acquired by means of an oscilloscope (Tektronix TSD2001C) using a high voltage probe and a resistor (223Ω) placed in series with the grounded electrode. The consumed power, $P(w)$, was calculated analysing the Lissajous figures (supplementary material S1 shows a sketch of the electrical connections).

The percentage of decomposed ammonia can be estimated as the difference between the ammonia moles in the inlet ($n_{\text{NH}_3}^{\text{in}}$) and outlet ($n_{\text{NH}_3}^{\text{out}}$) flows of the plasma reactor:

$$D(\%) = \frac{n_{\text{NH}_3}^{\text{in}} - n_{\text{NH}_3}^{\text{out}}}{n_{\text{NH}_3}^{\text{in}}} \cdot 100 \quad (1)$$

Hydrogen yield is expressed in terms of the amount of hydrogen produced per time unit, and is defined as:

$$H_2 \text{ yield} = \frac{3}{2} \cdot D \cdot Q_{NH_3}^{in} \tag{2}$$

where D is the decomposition rate defined above and $Q_{NH_3}^{in}$ is the total NH_3 flow rate feeding the reactor.

The specific energy input (SEI) and the energy efficiency (EE) parameters have been used to evaluate the efficiency of the process and are defined as follows:

$$SEI(kJ/L) = \frac{P(W) \cdot 60}{Q^{in}(sccm)} \tag{3}$$

$$EE(LH_2/kWh) = \frac{Q_{H_2}(sccm) \cdot 60}{P(W)} \tag{4}$$

where Q^{in} refers to the flow rate of NH_3 feeding the reactor and Q_{H_2} to the flow rate of produced H_2 . SIE accounts for the mean energy deposited per molecule in the reactor, while EE refers to the amount of hydrogen produced per unit of consumed energy.

Results and Discussion

Electrical Analysis of the Packed-Bed Reactor

A first step in this investigation was to evaluate the influence of the ammonia flow rate on the electrical behaviour of the reactor. Figure 2 shows the $I(t)$ curves obtained upon

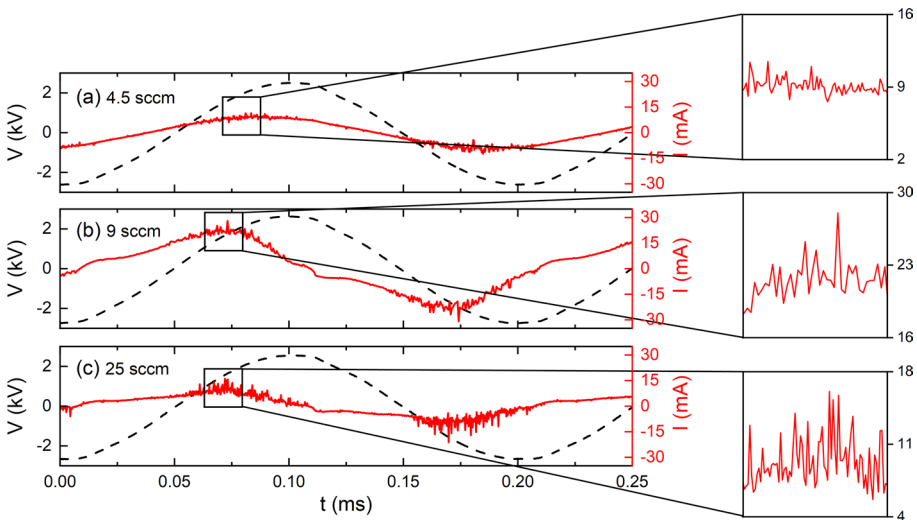


Fig. 2 $I(t)$ characteristic curves for an applied sinusoidal $V(t)$ voltage of 2.5 kV and 5 kHz of frequency for **a** 4.5 sccm, **b** 9 sccm and **c** 25 sccm NH_3 flow rates

applying a $V(t)$ sinusoidal signal of 2 kV amplitude and 5 kHz frequency and three NH_3 flow rates (4.5, 9 and 25 sccm). It is noticeable that $I(t)$ curves deviate from a sinusoidal behaviour as the flow rate increases and that the superimposed microdischarges are more intense and their density higher as the flow rate increases. For the 4.5, 9 and 25 sccm flow rates the mean microdischarge amplitude was 1.68, 2.55 and 3.62 mA, respectively. To estimate the microdischarge amplitude, we used a Fourier and filtering procedure, as detailed explained in supplementary material S2.

The Lissajous figures plotted in Fig. 3a correspond to the used flow rates and applied voltage, this latter varying from 1.5 to 2.5 kV. It appears that, at a constant flow rate, the higher the voltage the higher the transferred charge (there is a vertical enlargement of the charge–voltage curves in this figure) and consumed power (calculated as the area of the Lissajous plot multiplied by the frequency). It can be also realized that, as the flow rate increases, the shape of the curves evolves from circular or almond shapes to parallelepipedal, in agreement with the deformation of the $I(t)$ curves observed at high flow rates.

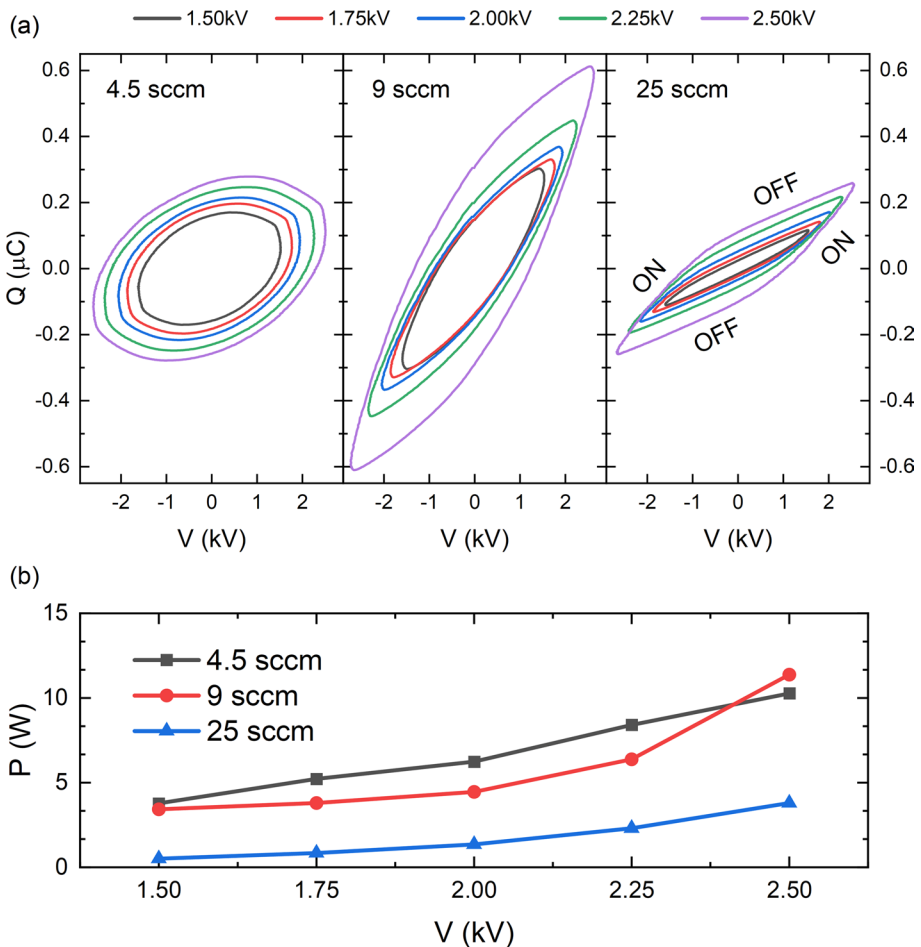


Fig. 3 **a** Lissajous figures and **b** consumed powers for different applied voltages (1.5, 1.75, 2, 2.25 and 2.5 kV) and flow rates (4.5, 9 and 25 sccm). Frequency was kept constant at 5 kHz for all experiments

For example, the 25 sccm case reveals that plasma on- and off- regions can be easily determined using the Lissajous figures [36]. The figures obtained for the 4.5 sccm flow reveal a clear capacitive component, unlike the shape of the curves obtained at higher flow rates. As discussed in next sections, we believe that this effect can be attributed to a surface chemical reduction experienced by the barium titanate pellets exposed to a hydrogen-rich plasma when working at high flow rates. Such a reduction would promote the occurrence of microdischarges, resulting in plasmas with a more resistive but less capacitive character at higher flows.

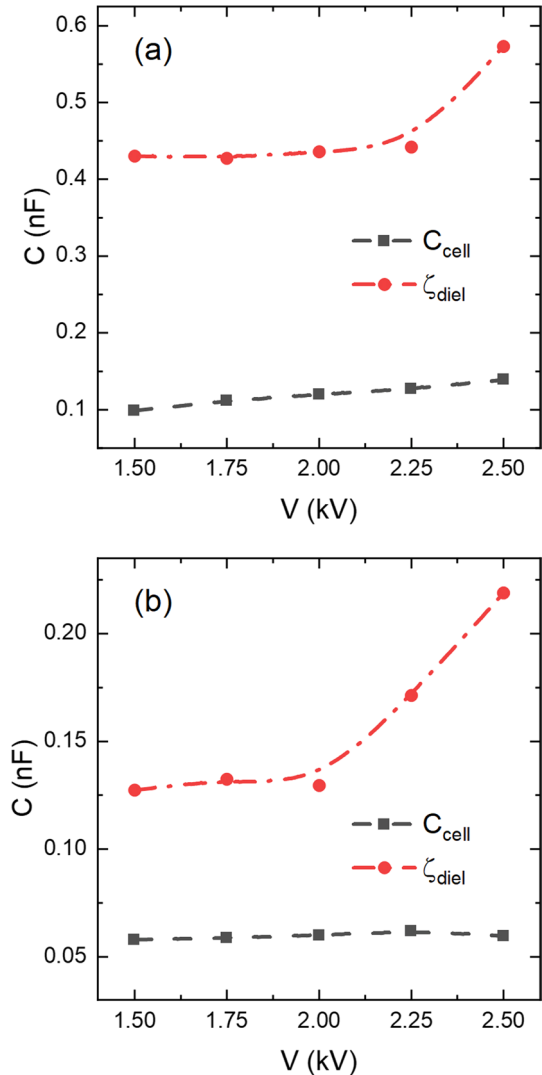
From the curves in Fig. 3a we estimated the consumed power, whose values are shown in Fig. 3b for the different operational conditions. Interestingly, at 25 sccm, despite the higher density and intensity of microdischarges, the consumed power was smaller than the one calculated for 4.5 and 9 sccm, these two conditions rendering similar values. This behaviour is a consequence of the $I(t)$ curve deformation shown in Fig. 2 and the smaller contribution of displacement current in the experiments using a flow of 25 sccm. From an electrical point of view, a higher microdischarge amplitude is a consequence of a lower plasma impedance at high flow rates. This feature can be attributed to changes in the properties of the BaTiO₃ ferroelectric packing bed material, as suggested above and further discussed later.

These electrical reactor responses can be interpreted on the basis of the equivalent circuit model proposed by Peeters and Sanden [37]. Following the premises of this model, the electrical effect of the discharge moderator is usually represented by a capacitor, C_{diel} . The capacitance of the barrier empty space is C_{gap} , while for the entire reactor in the absence of plasma the capacitance is represented by C_{cell} (it is worth mentioning that the capacitance of the gap varies when the gases proportions in the mixture change, as it is the case in our study due to the change in conversion rate for each examined flow). A variable resistor R represents the plasma consumed power. As shown in the supplementary material S3, the equivalent circuit of Peeters and Sanden [37] divides the interelectrode space into two regions, a first one filled with the plasma discharge (characterized by a unit ratio β) and another with no plasma (unit ratio α). For the entire reactor $\alpha + \beta = 1$. Since in our case the plasma does not occupy the whole interelectrode space, the dielectric capacity is better represented by ζ_{diel} instead of C_{diel} . ζ_{diel} is defined as indicated in Eq. 5 and, in partial discharges, corresponds to the slope of the plasma-on region of the Lissajous figure. The cell and dielectric capacitances (C_{cell} and ζ_{diel}) can be calculated from the slope of the ON- and OFF-regions of the Lissajous figures. For this purpose, we used a regression analysis, with a regression coefficient consistently above 0.98. Supplementary material S3 provides a detailed account about this analysis and calculations.

$$\zeta_{\text{diel}} = \alpha C_{\text{cell}} + \beta \cdot C_{\text{diel}} \quad (5)$$

Under our working conditions, although it is not possible to accurately estimate α and β (it would require that plasma fills the entire space between electrodes, but the reactor short-circuited when approaching this stage), we may analyse the relative variation of β (see Eq. 6). This relative variation would provide an approximate description of the plasma expansion as the voltage increases. In other words, although we cannot calculate the extension of the plasma discharge region, we may have information about how it increases/decreases following the evolution of the parameter β with the voltage.

Fig. 4 Capacitances calculated from Lissajous figures represented as a function of the external applied voltage for **a** 9 sccm and **b** 25 sccm of NH_3 . Note the different Y scales in each plot. Frequency 5 kHz



$$\frac{\Delta\beta}{\beta} \equiv \frac{\beta^{(2)} - \beta^{(1)}}{\beta^{(1)}} = \frac{\zeta_{\text{diel}}^{(2)} - \zeta_{\text{diel}}^{(1)}}{\zeta_{\text{diel}}^{(1)} - C_{\text{cell}}} \quad (6)$$

Figure 4 shows the C_{cell} and ζ_{diel} values determined for the 9 and 25 sccm reactant flow rates as a function of applied voltage (Fig. 3a shows that only the comparison of these two flow rates allow to clearly differentiate the ON- and OFF- plasma regions according to the equivalent circuit model). According to the plots in this figure, C_{cell} remains almost constant with approximate values of 0.11 and 0.06 for 9 sccm and 25 sccm flows, respectively. However, ζ_{diel} grows rather sharply for voltages higher than 2 kV, an increase that points to a dependence on some specific physical magnitudes. Firstly, the known variation in the dielectric constant of BaTiO_3 (and therefore C_{diel}) as the applied voltage increases

[33, 38]. Secondly, a possible change of C_{diel} if the surface of pellets becomes reduced by their exposure to a plasma rich in hydrogen and therefore with a highly reducing chemical character. Figure S4 in the supplementary material shows a photograph of an already used packed bed with the pellets depicting dark spots, which are attributed to a partial reduction of the surface. We assume that this reduction process contributes to vary the surface impedance of the pellets (they should be less resistive upon reduction), thus favouring the development of microdischarges. This assumption agrees with the higher density of microdischarges depicted in Fig. 2 for the 25 sccm flow. In this way, both an intensification of the microdischarges and an increase in the concentration of H_2 in the discharge volume will take place as the reduction degree of the surface of pellets progressively increases up to reach the steady state (we will come back to this point in next sections). As a third factor in this retrofitting scheme, we claim that an increase in β (Eq. (5)) occurs because plasma volume expands when operating voltage increases.

The relative variation of β , depicted in Fig. 5, confirms the hypothesis above. For both the 9 and 25 sccm flow rates, an increase in the discharge volume correlates with the increase in the amplitude of the applied voltage, but with a more pronounced effect for the 25 sccm flow rate. To a first approximation, this increase in the relative plasma volume will lead to an enhancement in the probability of electron-ammonia interaction and lead to an increase in the ammonia decomposition degree.

Decomposition Rate and Energy Efficiency

After the previous assessment of the electrical behaviour of the reactor, we analysed the gas outlet products, which solely consisted of N_2 and H_2 , along with unreacted NH_3 . No traces of hydrazine were detected in the conducted experiments (as proved by mass spectrometry, see supplementary material S5). This analysis proved that the gas flow composition at the reactor outlet is consistent with the NH_3 decomposition reaction $2NH_3 \rightarrow N_2 + 3H_2$, with no traces of other substances. Figure 6 shows the evolution of the percentage of NH_3 decomposition and that of the energy efficiency of the process as a function of the applied voltage for the three flow rates utilized in this work. In all cases (Fig. 6a) the decomposition of NH_3 is favoured at higher voltages, reaching a maximum of 14% at 4.5 sccm and 2.5 kV. The increasing evolution of the decomposition percentages vs. voltage was different depending on the flow rates: for 4.5 and 9 sccm the increase was around 10% per kV, while for 25 sccm it was around 4%. The values of these ratios are somehow contradictory with the electrical analysis of the reactor behaviour reported in the previous section, where

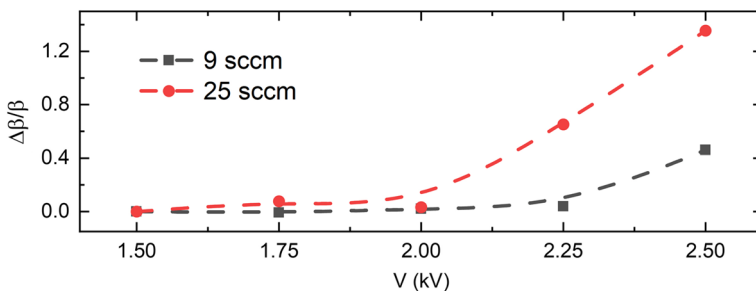
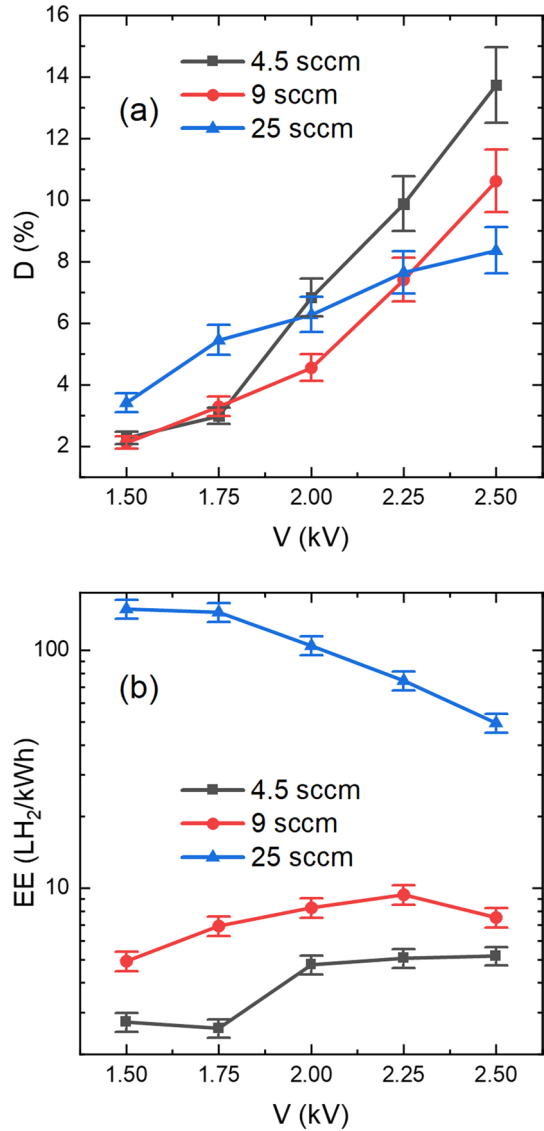


Fig. 5 Relative variation of the discharge volume as a function of the applied voltage for 9 and 25 sccm. Frequency 5 kHz

Fig. 6 **a** NH_3 decomposition percentage and **b** energy efficiency for different applied voltages and NH_3 flow rates



a higher plasma intensity was found for 25 sccm flow rate. In the same line, the curves of energy efficiency in Fig. 6b prove one order of magnitude enhancement in this parameter for the 25 sccm flow and all applied voltages (note the logarithmic scale in this plot). This result stresses the importance of properly adjusting the working parameters during operation of packed bed reactors. In the experiments herein, the development of a relatively large plasma volume and an enhancement in the density and intensity of microdischarges when operating the reactor at 25 sccm leads to a clear increase in energy efficiency [29]. Meanwhile, the much lower energy efficiency obtained for the 4.5 and 9 sccm flows must be attributed to that only part of the applied power (see Fig. 3b) is spent in the generation of microdischarges, the rest being spent in the form of displacement current.

Figure 6b also reveals that EE varies differently with voltage for the 25 sscm and the other two flows: in the former case efficiency decreases with voltage, while for 9 and 4.5 sscm it slightly increases. This result, together with the slow progression in decomposition rate at the highest flow (c.f. Figure 5a) mean that at 25 sscm and high voltages a significant fraction of the input energy is wasted in other processes that are inefficient to generate H_2 (i.e., NH_3 decomposition) [22, 34]. We suggest that at high flow rates and high power consumptions (i.e., for applied voltages above 1.75 kV), the amount of produced N_2 and H_2 is high enough to make quantitatively relevant the formation of NH_3 molecules. Reverse reactions are demonstrated to occur in different plasma-assisted chemical processes and are thought to be one of the factors bringing down the efficiency in packed-bed plasma reactions [22, 34]. To prove that this reaction is feasible under the utilized reaction conditions, new experiments were conducted with mixtures N_2 and H_2 and the same experimental conditions than for the NH_3 decomposition experiments. The results, shown as supplementary material S6, demonstrate the production of NH_3 , with nitrogen conversion rates of approximately 1.2% at 2.5 kV. This proves that under the experimental conditions of this study, the reverse reaction is likely to occur. It is noteworthy that, despite the considerable increase in the occurrence of back-reactions occurring for the 25 sscm experiment (and therefore a progressive decrease in the overall energy efficiency for the production of H_2), values as high as 50 LH_2/kWh are still obtained at 2.5 kV for the ammonia decomposition reaction.

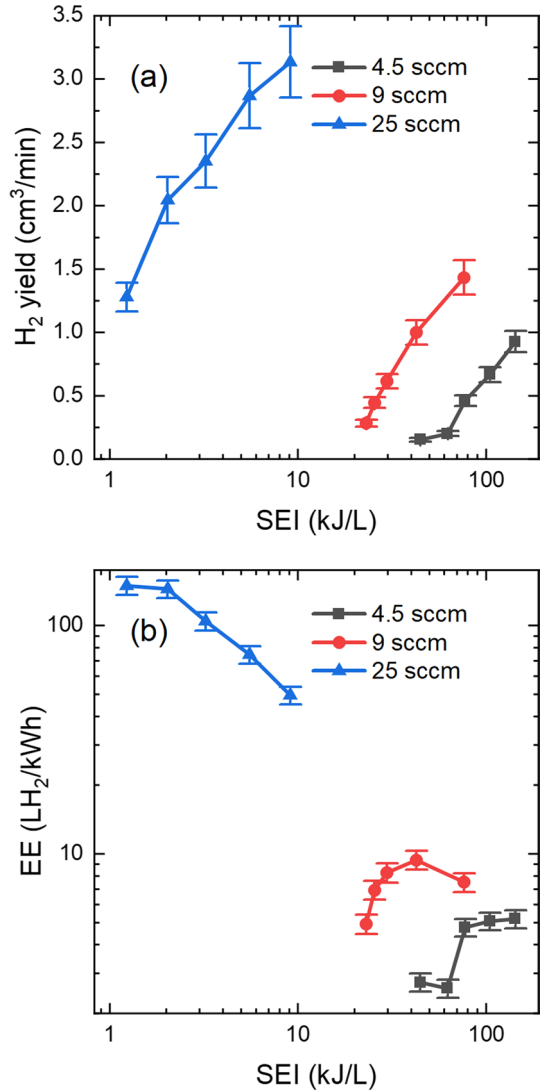
Parameters such as the total hydrogen production and specific energy input (SEI) are commonly used to figure out how energetic factors affect reactor performance. Figure 7 shows plots of hydrogen yield (in mLH_2/min) and EE as a function of SEI. Figure 7a shows that, for all analysed flow rates, the increase in the amount of energy deposited per molecule leads to an increase in the production of hydrogen. This is equivalent to say that the availability of more energy per molecule increases the probability of activating ammonia decomposition processes. It should be remarked that the same applies to back reactions, making that at high production rates the efficiency may relatively decrease as deduced when comparing the 25 sscm curves in Fig. 7a and b.

Bringing together the results in Fig. 5 about discharge volume variations and the data in Fig. 7, it can be realized that, for each flow rate, an increase in the specific energy input corresponds to an increase in the discharge volume. This means that there is a greater amount of energy available per molecule to decompose the ammonia, as well as to promote back reactions. In addition, part of the energy can be dissipated in the form of heat.

In general, to optimize the hydrogen production yield, a good trade-off between ammonia decomposition, hydrogen yield and energy efficiency should be found. Figure 8 shows the NH_3 decomposition rate as a function of EE. The maximum NH_3 decomposition of 14% found for a flow of 4.5 sscm corresponds to an efficiency of 10.4 LH_2/kWh . Data in our work also demonstrated that in our system varying the ammonia flow rate is a simple way to increase ammonia decomposition and energy efficiency. A flow rate of 4.5 sscm renders the maximum decomposition, which drastically decreased for higher flow rates of 25 sscm to values around 5–8%, though with an energy efficiency above 140 LH_2/kWh (and a higher hydrogen yield at a lower SEI as compared to 4.5 and 9 sscm flows). Thus, taking together the plots in Figs. 7 and 8, it can be deduced that most favourable conditions to establish an optimum trade-off between EE, H_2 -yield and decomposition percentage are a flow of 25 sscm and medium voltages. Recirculation of gases after recovering hydrogen (e.g., with palladium-platine membranes placed at the reactor outlet) would also contribute to optimize the reactor performance.

A final remark refers to heating effects that may be encountered during operation of ferroelectric reactors. One of the consequences of increasing power is reactor warming

Fig. 7 **a** H_2 production and **b** energy efficiency as a function of the specific energy input (SEI) for the three different flows used



(in fact, during long working periods at the highest powers the reactor reached a temperature of 40 °C, measured at the reactor wall). Considering that $BaTiO_3$ has a Curie temperature of 120 °C, and that a temperature drift inside the reactor is likely, there is a risk that moderator material loses its ferroelectric character at some contact-points and, thus, its ability to enhance plasma generation (the transition from ferroelectric to dielectric behaviour entails a drastic decrease in permittivity and, therefore, C_{diel}). This means that operating the reactor at low temperatures is crucial when working with $BaTiO_3$ as moderator. It is also likely that gas flow can be an important variable contributing to heat dissipation and, hence, to maintain the ferroelectric character of the discharge. The shape of the Lissajous curves in Fig. 3

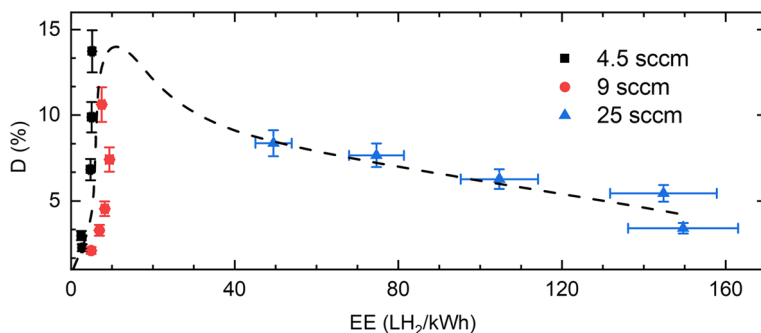


Fig. 8 Ammonia decomposition percentage as a function of the energy efficiency at a frequency of 5 kHz and the indicated flow rates

suggest such a transformation of the operating mode of the reactor when increasing the flow rate.

In relation to the chemical reduction of the surface of pellets discussed in the previous sections, we may assume that the resistivity of BaTiO₃ will decrease due to the reduction of pellets with a hydrogen rich plasma [39]. We assume that this reduction process contributes to reinforce the formation of microdischarges observed at high flows.

Benchmarking of Plasma Technologies and Other Hydrogen Production Technologies

The previous results and discussion gain relevance when comparing them with the latest results on ammonia decomposition in packed-bed plasma reactors and other types of discharges. Table 1 shows the percentage of ammonia decomposition, consumed power, ammonia input flow, energy costs, EE, and SEI values recently obtained in different works. It can be seen that non-thermal arc plasma reactors provide the best results in terms of cost and energy efficiency, with values exceeding 1000 LNH₃/kWh and 1500 LH₂/kWh. Additionally, they allow for the treatment of large gas flows. We should mention in this regard that arc reactors require large input flows to operate and that, therefore, they may not be suitable for situations where localized small-scale hydrogen production is needed. In these cases, packed-bed reactors would likely be a better choice. Induction reactors have also depicted good results in terms of NH₃ decomposition percentages, albeit with lower energy cost and efficiencies (energy costs are defined as LNH₃/kWh, so it is desirable for this value to be as high as possible). Our results are similar to those obtained by other authors using dielectric barrier discharge or packed-bed configuration reactors. We would like to highlight that our reactor is advantageous because it does not use any catalyst and operates at ambient conditions. This contrasts with most packed-bed reactor studies, where operating temperature exceeds 400 °C to make catalytic effects relevant. To increase energy efficiency with our reactor we foresee the implementation of selective membranes to remove H₂ from the discharge immediately after its formation and the possibility of operating by recirculating gas flows. The use of catalysts could also be beneficial, as well as redesigning the reactor by varying aspects such as the shape, size, and material of the pellets, as well as its characteristic dimensions.

Table 1 Recently obtained results for the ammonia decomposition process by means of plasma technologies

Comments and ref	NH ₃ descom. (%)	Power (W)	NH ₃ flow (sccm)	Energy cost (L _{NH₃} /kWh)	EE (L _{NH₃} /kWh)	SEI (kJ/L _{NH₃})
Gliding Arc. 50 Hz. Max. 8 kV and 100 mA. NH ₃ + Ar (180L/h, 5% of NH ₃) [40]	42	175	150	21.60	32.40	3.50
Gliding Arc. 50 Hz. Max. 8 kV and 100 mA. NH ₃ + Ar (180L/h, 5% of NH ₃) [40]	70	325	150	19.38	29.08	6.50
DBD. Cu rod electrode. 50 kHz and 5 kV % NH ₃ = 4.87% in N ₂ 100-200 mL/min [30]	100	140	7.3	3.13	4.70	56.00
DBD. Fe rod electrode. 50 kHz and 5 kV % NH ₃ = 4.87% in N ₂ 100-200 mL/min [30]	100	100	7.3	4.38	6.57	40.00
DBD. Hydrogen separation membrane. Quartz reactor. 14 kV and 90 kPa permeation pressure [24]	23	200	5000	345.00	517.50	2.40
Catalytic reactor + DBD. 700 °C and 110 V. Power heater 175W and hydrogen separation pump 150W [25]	74.1	325	90	12.31	18.46	216.67
NTAP (non-thermal arc plasma) [41]	30.5	700	30,000	783.40	1175.10	1.40
NTAP+catalyst [41]	42	700	30,000	1080.00	1620.00	1.40
Quartz reactor. Induction plasma reactor [42]	98.7	25,000	14,000	33.16	49.74	107.14
Quartz reactor. Induction plasma reactor [42]	91.3	25,000	27,000	59.16	88.74	55.56
Packed-bed plasma reactor with Fe-Ni catalysts 500 °C and 10 kHz [27]	99.9	48.2	120	149.23	223.84	24.10
Packed-bed reactor. Without catalyst. Room temperature [22]	17	23	9	3.99	5.99	153.33
Packed-bed reactor. Without catalyst. Room temperature [22]	12	9	5	4.00	6.00	108.00
Packed-bed reactor. Input power 45 W (without furnace heating) 100 mL/min at 550 °C [26]	90	45	100	120.00	180.00	27.00
DBD.470 °C [28]	9.7	33.83	40	6.88	10.32	50.76
DBD + Fe catalyst. 410 °C [28]	100	30.24	40	79.36	119.04	45.36
Packed-bed. Only Plasma (3 kHz, 4.5 mm gap) [29]	5	21	75	10.71	16.07	16.80
Packed-bed + catalyst (MgAl ₂ O ₄) (3 kHz, 4.5 mm gap) [29]	13	21	75	27.86	41.79	16.80
DBD. 600 K. 1000 sccm 1% NH ₃ in N ₂ [31]	15	20	10	4.50	6.75	120.00
This work. Packed-bed reactor without catalyst. Room temperature and atmospheric pressure	14.0	10.7	4.5	6.9	10.4	143
This work. Packed-bed reactor without catalyst. Room temperature and atmospheric pressure	11.0	11.4	9	5.0	7.5	76.3
This work. Packed-bed reactor without catalyst. Room temperature and atmospheric pressure	8.4	3.8	25	33.0	49.5	9.12
This work. Packed-bed reactor without catalyst. Room temperature and atmospheric pressure	3.5	0.51	25	100.0	150	1.22

By the Net Zero Emission Scenario in 2050, the cost of H_2 should ideally remain within the range of \$1–2 per kilogram(H_2), which corresponds to approximately 60 g(H_2)/kWh [43] (under normal conditions, it is around 672 g(H_2)/kWh). This means that further research is still required to achieve this target, and that emerging plasma technologies are still far but approaching this desired value [31]. Other technologies at more advanced TRL (Technology readiness level) are beginning to be implemented in industrial applications. For instance, electrolysis achieves yields of approximately 600–10000 L_{H_2} /kWh [44, 45] and microwave assisted production values of 149 L_{H_2} /kWh [43, 46]. Catalytic processes, which are responsible for the majority of H_2 currently produced, boast conversion rates exceeding 99% [47–50]. Plasma technology is still at a low TRL level and therefore requires of further research. Owing to its operational advantages (zero emissions, minimal wastes, the ability to operate under normal pressure and temperature conditions, and in a distributed manner, etc.), overcoming current bottlenecks hindering high yields and conversions is a clear challenge to make plasma competitive with other procedures.

Conclusions

In this work we have shown that a FBD reactor moderated with $BaTiO_3$ pellets and no catalyst is rather effective to promote the decomposition of ammonia into hydrogen and nitrogen at ambient temperature and relatively low activation voltages and frequencies. The effectiveness of the process has been compared with the plasma conditions of the discharge, finding a good correlation between reaction parameters, such as decomposition rate and energy efficiency, with plasma parameters, such as volume and density of the plasma in the interpellet space and the consumed power of the discharge. Although some surface contribution to the decomposition rate cannot be discarded at this point, experimental results suggest that the characteristics of the plasma discharge is the primary factor controlling the efficiency of the process. In this scenario, hints exist about that a back reaction between N_2 and H_2 to yield NH_3 can be detrimental and contribute to decrease the yield for the ammonia decomposition reaction. This suggests that an immediate removal of hydrogen from the reaction medium (e.g., using Pd–Pt membranes) would be desirable to optimize the plasma technology to decompose ammonia.

By the analysis of the electrical characteristics of the plasma discharge it has been found that the flow rate of reactants contributes to increase the plasma intensity. This unexpected result has been tentatively explained assuming that at low temperatures the surface of the $BaTiO_3$ pellets may be partially reduced (i.e., $Ti^{4+} \rightarrow Ti^{3+}$) by the interaction with the reducing plasma and that a discharge intensification benefits from this chemical reduction of the surface of pellets, now formed by an unmodified ferroelectric core and a very thin crust with less electrical resistivity. Another possible factor contributing to reinforce the intensity of the discharge at high flow rates is heat removal from the plasma zone and the preservation of the ferroelectric properties of the pellets.

Supplementary Information The online version contains supplementary material available at <https://doi.org/10.1007/s11090-023-10427-7>.

Authors' Contribution MRM: Investigation and formal analysis. SMM: Investigation. AMS: Investigation. MOR: formal analysis. JC: Conceptualization. ARGE: Conceptualization, methodology, formal analysis, and writing—review and editing. AGR: Conceptualization, formal analysis, conceptualization and methodology, writing—review and editing, supervision, project administration, and funding acquisition. All authors reviewed the manuscript.

Funding Funding for open access publishing: Universidad de Sevilla/CBUA. The authors acknowledge projects PID2020-114270RA-I00, and PID2020-112620GB-I00 funded by MCIN/AEI/10.13039/501100011033, project TED2021-130124A-I00 funded by AEI/10.13039/501100011033/ Unión Europea Next Generation EU/PRTR and projects P18-RT-3480, US-1381045, and US-1380977 funded by Conserjería de Economía, Conocimiento, Empresas y Universidad de la Junta de Andalucía (PAIDI-2020) and Programa Operativo Feder 2014-2020. M. Oliva-Ramírez acknowledges financial support from Grant IJC2020-045087-I funded by: MCIN/ AEI /10.13039/501100011033 and the European Union NextGeneration EU /PRTR and S. Marín Meana acknowledges financial support from Grant PRE2021-100465 funded by MCIN/AEI/10.13039/501100011033 and FSE+.

Availability of Data and Materials Data are available upon request to the corresponding author.

Declarations

Conflict of interest The authors have no competing interests as defined by Springer, or other interests that might be perceived to influence the results and/or discussion reported in this paper.

Ethical Approval Not applicable.

Open Access This article is licensed under a Creative Commons Attribution 4.0 International License, which permits use, sharing, adaptation, distribution and reproduction in any medium or format, as long as you give appropriate credit to the original author(s) and the source, provide a link to the Creative Commons licence, and indicate if changes were made. The images or other third party material in this article are included in the article's Creative Commons licence, unless indicated otherwise in a credit line to the material. If material is not included in the article's Creative Commons licence and your intended use is not permitted by statutory regulation or exceeds the permitted use, you will need to obtain permission directly from the copyright holder. To view a copy of this licence, visit <http://creativecommons.org/licenses/by/4.0/>.

References

1. IPCC reports. AR6 synthesis report: climate change 2023. <https://www.ipcc.ch/report/sixth-assessment-report-cycle/>
2. https://commission.europa.eu/strategy-and-policy/priorities-2019-2024/european-green-deal_es
3. Rouwenhorst KHR, Engelmann Y, Van't Veer K, Postma RS, Bogaerts A, Lefferts L (2020) Plasma-driven catalysis: green ammonia synthesis with intermittent electricity. *Green Chem* 22(19):6258–6287. <https://doi.org/10.1039/D0GC02058C>
4. Salmon N, Bañares-Alcántara R (2021) Green ammonia as a spatial energy vector: a review. *Sustain Energy Fuels* 5(11):2814–2839. <https://doi.org/10.1039/D1SE00345C>
5. Preuster P, Albert J (2018) Biogenic formic acid as a green hydrogen carrier. *Energ Technol* 6(3):501–509. <https://doi.org/10.1002/ente.201700572>
6. Teichmann D, Arlt W, Wasserscheid P (2012) Liquid organic hydrogen carriers as an efficient vector for the transport and storage of renewable energy. *Int J Hydrogen Energy* 37(23):18118–18132. <https://doi.org/10.1016/j.ijhydene.2012.08.066>
7. Valera-Medina A, Bañares-Alcántara R (2021) Chapter 1 Introduction. In: Valera-Medina A, Bañares-Alcántara R (eds) *Techno- economic challenges of green ammonia as an energy vector*. Academic Press, pp 1–14
8. Hu X-C, Wang W-W, Jin Z, Wang X, Si R, Jia C-J (2019) Transition metal nanoparticles supported La-promoted MgO as catalysts for hydrogen production via catalytic decomposition of ammonia. *J Energy Chem* 38:41–49. <https://doi.org/10.1016/j.jechem.2018.12.024>
9. Benés M, Pozo G, Abián G, Millera Á, Bilbao R, Alzueta MU (2021) Experimental study of the pyrolysis of NH₃ under flow reactor conditions. *Energy Fuels* 35(9):7193–7200. <https://doi.org/10.1021/acs.energyfuels.0c03387>
10. Little DJ, Smith Milton III, Hamann TW (2015) Electrolysis of liquid ammonia for hydrogen generation. *Energy Environ Sci* 8(9):2775–2781. <https://doi.org/10.1039/C5EE01840D>
11. Lee JS, Han G-F, Baek J-B (2023) Mechanochemical ammonia synthesis: old is new again. *ChemSuschem*. <https://doi.org/10.1002/cssc.202300459>

12. Maslova V et al (2023) Ammonia decomposition in electric field over Ce-based materials. *Chem-CatChem* 15(4):e202201626. <https://doi.org/10.1002/cctc.202201626>
13. Kogelschatz U (2003) Dielectric-barrier discharges: their history, discharge physics, and industrial applications. *Plasma Chem Plasma Process* 23(1):1–46. <https://doi.org/10.1023/A:1022470901385>
14. Bogaerts A, Neyts EC, Guaitella O, Murphy AB (2022) Foundations of plasma catalysis for environmental applications. *Plasma Sources Sci Technol* 31(5):053002. <https://doi.org/10.1088/1361-6595/ac5f8e>
15. Navascués P, Cotrino J, González-Elipse AR, Gómez-Ramírez A (2022) Plasma assisted CO₂ dissociation in pure and gas mixture streams with a ferroelectric packed-bed reactor in ambient conditions. *Chem Eng J* 430:133066. <https://doi.org/10.1016/j.cej.2021.133066>
16. Chen HL, Lee HM, Chen SH, Chao Y, Chang MB (2008) Review of plasma catalysis on hydrocarbon reforming for hydrogen production: Interaction, integration, and prospects. *Appl Catal B* 85(1):1–9. <https://doi.org/10.1016/j.apcatb.2008.06.021>
17. Navascués P, Cotrino J, González-Elipse AR, Gómez-Ramírez A (2023) Plasma assisted dry reforming of methane: syngas and hydrocarbons formation mechanisms. *Fuel Process Technol* 248:107827. <https://doi.org/10.1016/j.fuproc.2023.107827>
18. Chen HL, Lee HM, Chen SH, Chang MB (2008) Review of packed-bed plasma reactor for ozone generation and air pollution control. *Ind Eng Chem Res* 47(7):2122–2130. <https://doi.org/10.1021/ie071411s>
19. Wang Y et al (2022) Shielding protection by mesoporous catalysts for improving plasma-catalytic ambient ammonia synthesis. *J Am Chem Soc* 144(27):12020–12031. <https://doi.org/10.1021/jacs.2c01950>
20. Gomez-Ramirez AC, Lambert RM, Gonzalez-Elipse AR (2015) Efficient synthesis of ammonia from N₂ and H₂ alone in a ferroelectric packed-bed DBD reactor. *Plasma Sour Sci Technol* 24(6):65011. <https://doi.org/10.1088/0963-0252/24/6/065011>
21. Navascués P, Garrido-García J, Cotrino J, González-Elipse AR, Gómez-Ramírez A (2023) Incorporation of a metal catalyst for the ammonia synthesis in a ferroelectric packed-bed plasma reactor: Does it really matter? *ACS Sustain Chem Eng* 11(9):3621–3632. <https://doi.org/10.1021/acssuschemeng.2c05877>
22. Navascués P, Obrero-Pérez JM, Cotrino J, González-Elipse AR, Gómez-Ramírez A (2020) Unraveling discharge and surface mechanisms in plasma-assisted ammonia reactions. *ACS Sustain Chem Eng* 8(39):14855–14866. <https://doi.org/10.1021/acssuschemeng.0c04461>
23. Rouwenhorst KHR, Burbach HGB, Vogel DW, Núñez Paulí J, Geerdink B, Lefferts L (2021) Plasma-catalytic ammonia synthesis beyond thermal equilibrium on Ru-based catalysts in non-thermal plasma. *Catal Sci Technol* 11(8):2834–2843. <https://doi.org/10.1039/D0CY02189J>
24. Hayakawa Y, Kambara S, Miura T (2020) Hydrogen production from ammonia by the plasma membrane reactor. *Int J Hydrogen Energy* 45(56):32082–32088. <https://doi.org/10.1016/j.ijhydene.2020.08.178>
25. Hayakawa Y, Miura T, Shizuya K, Wakazono S, Tokunaga K, Kambara S (2019) Hydrogen production system combined with a catalytic reactor and a plasma membrane reactor from ammonia. *Int J Hydrogen Energy* 44(20):9987–9993. <https://doi.org/10.1016/j.ijhydene.2018.12.141>
26. Wang L, Yi Y, Guo Y, Zhao Y, Zhang J, Guo H (2017) Synergy of DBD plasma and Fe-based catalyst in NH₃ decomposition: plasma enhancing adsorption step. *Plasma Process Polym* 14(6):1600111. <https://doi.org/10.1002/ppap.201600111>
27. Yi Y, Wang L, Guo Y, Sun S, Guo H (2019) Plasma-assisted ammonia decomposition over Fe–Ni alloy catalysts for CO x-free hydrogen. *AIChE J* 65(2):691–701. <https://doi.org/10.1002/aic.16479>
28. Wang L, Zhao Y, Liu C, Gong W, Guo H (2013) Plasma driven ammonia decomposition on a Fe-catalyst: eliminating surface nitrogen poisoning. *Chem Commun* 49(36):3787–3789. <https://doi.org/10.1039/C3CC41301B>
29. Andersen JA, Christensen JM, Østberg M, Bogaerts A, Jensen AD (2022) Plasma-catalytic ammonia decomposition using a packed-bed dielectric barrier discharge reactor. *Int J Hydrogen Energy* 47(75):32081–32091. <https://doi.org/10.1016/j.ijhydene.2022.07.102>
30. Akiyama M, Aihara K, Sawaguchi T, Matsukata M, Iwamoto M (2018) Ammonia decomposition to clean hydrogen using non-thermal atmospheric-pressure plasma. *Int J Hydrogen Energy* 43(31):14493–14497. <https://doi.org/10.1016/j.ijhydene.2018.06.022>
31. Bang S, Snoeckx R, Cha MS (2023) Kinetic study for plasma assisted cracking of NH₃: approaches and challenges. *J Phys Chem A* 127(5):1271–1282. <https://doi.org/10.1021/acs.jpca.2c06919>
32. Ndayirinde C et al (2023) Plasma-catalytic ammonia synthesis: Packed catalysts act as plasma modifiers. *Catal Today* 419:114156. <https://doi.org/10.1016/j.cattod.2023.114156>

33. Gómez-Ramírez A et al (2021) Electrical and reaction performances of packed-bed plasma reactors moderated with ferroelectric or dielectric materials. *Plasma Process Polym* 18(3):2000193. <https://doi.org/10.1002/ppap.202000193>
34. Navascués P, Obrero-Pérez JM, Cotrino J, González-Elipe AR, Gómez-Ramírez A (2019) Isotope labelling for reaction mechanism analysis in DBD plasma processes. *Catalysts* 9(1):9–11. <https://doi.org/10.3390/catal9010045>
35. Gómez-Ramírez A, Montoro-Damas AM, Rodríguez MA, González-Elipe AR, Cotrino J (2017) Improving the pollutant removal efficiency of packed-bed plasma reactors incorporating ferroelectric components. *Chem Eng J* 314:311–319. <https://doi.org/10.1016/j.cej.2016.11.065>
36. Pipa AV, Brandenburg R (2019) The equivalent circuit approach for the electrical diagnostics of dielectric barrier discharges: the classical theory and recent developments. *Atoms*. <https://doi.org/10.3390/atoms7010014>
37. Peeters FJJ, van de Sanden MCM (2015) The influence of partial surface discharging on the electrical characterization of DBDs. *Plasma Sources Sci Technol* 24(1):015016. <https://doi.org/10.1088/0963-0252/24/1/015016>
38. Li H, Subramanyam G (2009) Capacitance of thin-film ferroelectrics under different drive signals. *IEEE Trans Ultrason Ferroelectr Freq Control* 56(9):1861–1867. <https://doi.org/10.1109/TUFFC.2009.1262>
39. Sohrabi Baba Heidary D, Randall CA (2015) Analysis of the degradation of BaTiO₃ resistivity due to hydrogen ion incorporation: Impedance spectroscopy and diffusion analysis. *Acta Mater* 96:344–351. <https://doi.org/10.1016/j.actamat.2015.05.026>
40. Młotek M, Perron M, Krawczyk K (2021) Ammonia decomposition in a gliding discharge plasma. *Energy Technol* 9(12):2100677. <https://doi.org/10.1002/ente.202100677>
41. Lin QF et al (2021) Instantaneous hydrogen production from ammonia by non-thermal arc plasma combining with catalyst. *Energy Rep* 7:4064–4070. <https://doi.org/10.1016/j.egy.2021.06.087>
42. Soucy G, Jurewicz JW, Boulos MI (1995) Parametric study of the decomposition of NH₃ for an induction plasma reactor design. *Plasma Chem Plasma Process* 15(4):693–710. <https://doi.org/10.1007/BF01447067>
43. Hrycak B, Mizeraczyk J, Czyłkowski D, Dors M, Budnarowska M, Jasiński M (2023) Hydrogen production by the steam reforming of synthetic biogas in atmospheric-pressure microwave (915 MHz) plasma. *Sci Rep* 13(1):2204. <https://doi.org/10.1038/s41598-023-29433-y>
44. Modisha P, Bessarabov D (2016) Electrocatalytic process for ammonia electrolysis: a remediation technique with hydrogen co-generation. *Int J Electrochem Sci* 11:6627–6635. <https://doi.org/10.20964/2016.08.54>
45. Bhandari R, Trudewind CA, Zapp P (2014) Life cycle assessment of hydrogen production via electrolysis: a review. *J Clean Prod* 85:151–163. <https://doi.org/10.1016/j.jclepro.2013.07.048>
46. Chehade G, Lytle S, Ishaq H, Dincer I (2020) Hydrogen production by microwave based plasma dissociation of water. *Fuel* 264:116831. <https://doi.org/10.1016/j.fuel.2019.116831>
47. Li L, Wang Y, Xu ZP, Zhu Z (2013) Catalytic ammonia decomposition for CO-free hydrogen generation over Ru/Cr₂O₃ catalysts. *Appl Catal A Gen* 467:246–252. <https://doi.org/10.1016/j.apcata.2013.07.003>
48. Fu E et al (2021) Enhanced NH₃ decomposition for H₂ production over bimetallic M(M=Co, Fe, Cu) Ni/Al₂O₃. *Fuel Process Technol* 221:106945. <https://doi.org/10.1016/j.fuproc.2021.106945>
49. Lucentini I, Casanovas A, Llorca J (2019) Catalytic ammonia decomposition for hydrogen production on Ni, Ru and NiRu supported on CeO₂. *Int J Hydrogen Energy* 44(25):12693–12707. <https://doi.org/10.1016/j.ijhydene.2019.01.154>
50. Ohtsuka Y, Xu C, Kong D, Tsubouchi N (2004) Decomposition of ammonia with iron and calcium catalysts supported on coal chars. *Fuel* 83(6):685–692. <https://doi.org/10.1016/j.fuel.2003.05.002>

Publisher's Note Springer Nature remains neutral with regard to jurisdictional claims in published maps and institutional affiliations.